Hindawi
Journal of Nanomaterials
Volume 2021, Article ID 5533845, 8 pages
https://doi.org/10.1155/2021/5533845

Research Article

A Comparative Study of Nanostructures of CuO/Cu_2O Fabricated via Potentiostatic and Galvanostatic Anodization

S. Mary Margaret, Albin John P. Paul Winston, S. Muthupandi, P. Shobha, and P. Sagayaraj

Department of Physics, Loyola College (Autonomous), Chennai, Tamilnadu, India

Correspondence should be addressed to P. Sagayaraj; sagayaraj1962@gmail.com

Received 20 January 2021; Accepted 26 July 2021; Published 14 August 2021

Academic Editor: Joice Sophia Ponraj

A detailed comparative study on the synthesis process of coral-like CuO/Cu_2O nanorods (NRs) and nanopolycrystals (NPCs) fabricated on Cu foil employing aqueous electrolyte via potentiostatic (POT) and galvanostatic (GAL) modes is discussed. The structural, morphological, thermal, compositional, and molecular vibration of the prepared CuO/Cu_2O nanostructures was characterized by XRD, HRSEM, TG/DTA, FTIR, and EDX techniques. XRD analysis confirmed the crystalline phase of the formation of monoclinic CuO and cubic Cu_2O nanostructures with well-defined morphology. The average particle size was found to be 21.52 nm and 26.59 nm for NRs (POT) and NPCs (GAL), respectively, and this result is corroborated from the HRSEM analysis. POT synthesized nanoparticle depicted a higher thermal stability up to 600°C implying that the potentiostatically grown coral-like NRs exhibit a good crystallinity and well-ordered morphology.

1. Introduction

Development of efficient energy storage devices has gained a tremendous attention in recent years and. In this scenario, supercapacitors are emerging electrochemical energy storing devices due to its enormous properties like high power density, safe operational quality, fast charging/discharging rate, faster response time, long-term cycle stability and ecofriendliness [1–8]. Transition metal oxide/hydroxide such as CoO [9, 10], RuO_2 [11], NiO [12, 13], MgO, CuO [14–18], TiO_2 [19, 20], and FeO [21, 22] is the most commonly used electrode material in a electrochemical setup, and they determine the electrochemical performance of the supercapacitors [23]. Among these transition metal oxides, CuO is a multifunctional material, and it has versatile properties like inexpensiveness, low-toxicity, high theoretical capacity (670 $mAhg^{-1}$), and low electrical conductivity [24–26].

The two forms of Cu, namely, cuprous oxide (Cu_2O) that has a bandgap of ~2.17 eV and copper oxide (CuO) that has a bandgap of ~1.2–1.5 eV, are identified as excellent p-type semiconductors. Therefore, these materials can be used as electrodes in supercapacitors [27, 28], infrared photo detectors [29], lithium ion batteries [30], and photovoltaic solar cells [31]. Previous studies have been stimulated by these excellent properties to synthesizeCuO-Cu_2O nanoparticles [32]. It is evident from literature reviews that the bicomponent functional materials have improved the properties of super capacitors to greater extent than those of single component with morphologies such as CuO-Cu_2O nanowires [33], CuO-Cu_2O microspheres [34], nanorods [35, 36], CuO-Cu_2O nano-flowers [36], Leaf-Like CuO-Cu_2O [37], Cu_2O films [38], nanoribbons [39], Cu_2O nanocorals [40], and Cu_2O polycrystal [41]. The widely used processing routes among the various methods reported in the literature to fabricate CuO-Cu_2O are the hydrothermal method, electrochemical deposition [42], electrostatic spray deposition (ESD), sonochemical methods [43], and chemical bath method.

The one-step electrochemical deposition method is adopted for the fabrication of CuO/Cu_2O in the present work because

(i) It is a low-temperature growth process

(ii) Unbinding structure [44]

(iii) Constant temperature bath maintenance during phase composition

(iv) pH dependant

(v) Low applied potential to attain high degree of crystalline

(vi) High conductivity [45]

Although CuO/Cu_2O is abundant in nature, the most challenging issue is that they are highly unstable in aqueous phases. An attempt is therefore made in the present work to study the formation mechanism of CuO/Cu_2O nanostructures with various morphologies on Cu surface based on potentiostatic (POT) and galvanostatic(GAL) modes in NaOH, an aqueous electrolyte with pH ≥ 10 [46]. The comparative study fascinatingly helps to identify the prominent structures in which large amount of electrons could be packed into a small surface area that may help promoting the applications of the super capacitors.

2. Experimental Details

2.1. Materials. All the chemicals are of analytical grade and were used without further purification. High-purity copper foil (99.99%, 0.25 mm thick) was purchased from Sigma-Aldrich. NaOH from (Merck, India). Deionized water (DI) was obtained from the Deionizer Millipore Simplicity UV system, alumina powder has been procured from Merck, and acetone (99.5% purity), isopropyl alcohol (98% purity), and ethanol (96% purity) were purchased from Sigma-Aldrich. Hydrochloric acid (37%) was purchased from Emplura Merck. Pt mesh was bought from Sigma-Aldrich.

2.2. Synthesis of CuO/Cu_2O Coral-like Nanorods and Nanopolycrystals. Copper foil was uniformly cut into small pieces in the dimension of $2 \times 1\ cm^2$ and then polished with 0.2 μm alumina powder for the removal of the native oxide followed by a DI water rinse. Cu foils were ultrasonically cleaned in acetone, isopropyl alcohol, ethanol, and deionized water consecutively for 15 min and then immersed in 1.0 mold m^{-3} of HCL (35%) solution to remove surface impurities. The surface of the copper foil turned bright and smooth after the treatment. The precleaned Cu foils were then dried in air, and teflon tape was used to cover for one-sided anodization. In typical synthesis procedure, potentiostatic (POT) and galvanostatic (GAL) anodization was performed using two-electrode cell with Cu foil as the working electrode (WE). Pt mesh was used as a counter electrode (CE), and 1 M NaOH aqueous solution is used as electrolyte. Elico pH meter was used to confirm the alkaline nature (pH =12).

The working electrode and the counter electrode are placed at a constant distance of 3 cm to provide better dissemination of heat formed at the bottom of the pores. The distance between the WE and CE is maintained in order to attain a highly ordered pore diameter, wall thickness, and rod dimension. During the anodization process, a constant voltage of about 20 V and a constant current density of about 10 mA cm^{-2} were set to using Keithley 2400 as DC power source for both POT and GAL approaches, respectively. The anodization took place for 480 seconds at room temperature (~28°C). Once the anodization time is complete, the foil was cleaned with ethanol to obtain the exfoliated nanoparticles. Subsequently, the amorphous samples were then crystallized by annealing at 350°C for 1 hour. Finally, a black colored uniform film on the Cu foils is obtained which was taken for further characterizations.

2.3. Instrumentation. The structure, phase, and crystalline of the CuO/Cu_2O of POT and GAL were investigated by the X-ray diffraction system (Bruker XRD 3003 TT) using monochromatic nickel filtered CuK_α ($\lambda = 1.5406$ Å) radiation. The Fourier transform infrared (FT-IR) spectral analysis was carried out using a Perkin Elmer Spectrum Two. Scanning electron microscope (SEM Quanta 200 FEG) was employed for morphological study. The instrument is attached with an energy dispersive X-ray spectrometry (EDX) for performing crystalline information from the few nanometer depths of the material surface.

3. Results and Discussion

Figure 1 illustrates the one-step electrochemical anodization process of fabricating the CuO/Cu_2O on Cu electrode. Under the effect of POT and GAL, the copper substrate was made to oxidize and release Cu^{2+} and Cu^{+} ions into the NaOH solution respectivley, while OH^- in the solution captured the Cu^{2+} and Cu^{+} ions to form $Cu(OH)_2$ and CuOH nuclei with the following reactions [31],

$$Cu \xrightarrow{\text{anodization}} Cu_2{}^{+} + 2e^{-}, \tag{1}$$

$$Cu \xrightarrow{\text{anodization}} Cu^{+} + e^{-}. \tag{2}$$

During the process of anodization, the Cu surface on interaction with the OH^- ions that form the electrolyte under the influence of potential will change from the brown color to a faint blue color due to the formation copper II hydroxide. Cuprate ions in the form of the complex $Cu(OH)_2{}^{-4}$ were generated at the substrate–electrolyte interface, which creates nucleating sites on the copper substrate. Because of the negative charge on $Cu(OH)_2{}^{-4}$, it gets attracted rapidly toward the copper anode, where this combination precipitates the creation of the $Cu(OH)_2$ film on Cu at the anode. The obtained copper hydroxide film being crystalline is engineered to enhance the band gap or the phase formation by calcination in the presence of oxygen to yield a black precipitate indicating the presence of both CuO and Cu_2O [6, 45, 47].

$$Cu^{2+} + OH^{-} \longrightarrow Cu(OH)_2\{\text{anode}\}, \tag{3}$$

$$Cu^{+} + OH^{-} \longrightarrow Cu(OH), \tag{4}$$

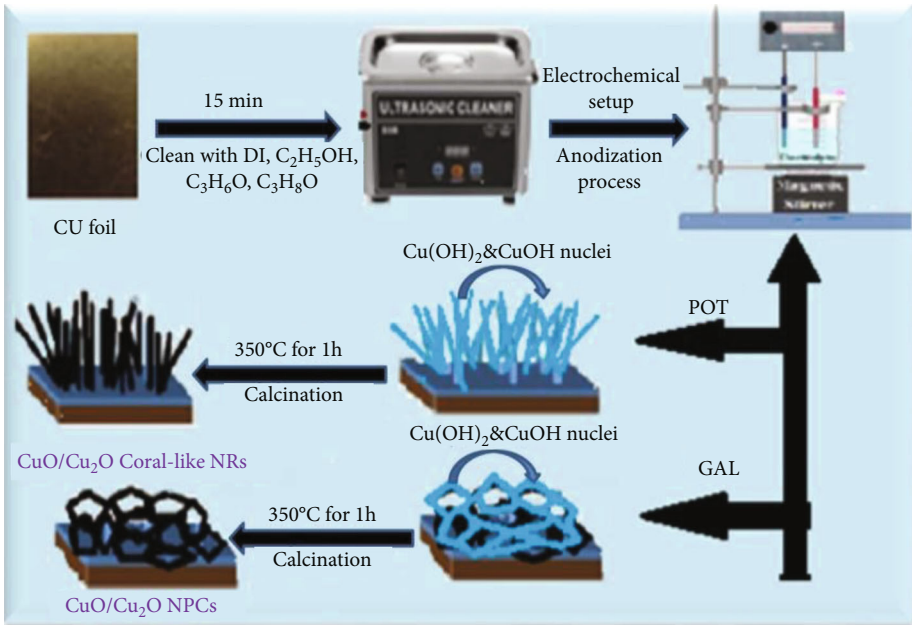

Figure 1: Schematic representation of fabrication of coral-like CuO/Cu_2O (NRs) and CuO/Cu_2O (NPCs) on Cu substrate.

$$Cu(OH)_2 \longrightarrow CuO + H_2O, \quad (5)$$

$$CuOH \longrightarrow Cu_2O + \frac{1}{2}H_2O. \quad (6)$$

XRD studies were carried out in order to understand the structural property of the prepared samples. The phase identification of a crystalline material and crystal structure of the *as*-prepared CuO-Cu_2O POT and GAL were analyzed by the XRD (Figure 2). The four peaks marked with diamond shape which can be indexed to the (111), (200), (111), and (-311) planes are presented in (Figure 2(a) and 2(b)) of the cubic Cu substrate (JCPDS No. 01-1241). The peaks are marked with clover shape which can be perfectly indexed to (002), (111), (-202), (202), (-311), and (220) planes of monoclinic CuO (JCPDS no. 89-2530), while the peaks marked with spade shape that can be indexed to the (111), (200), and (220) are the planes of the cubic Cu_2O (JCPDS no.77-0199), and no other crystalline peaks of impurities were observed which indicates that the *as*-prepared sample was highly pure. By using the Debye Scherrer formula, we could find average crystallite size (d) is calculated for both POT and GAL and was found to be ~21.52 nm and~26.59 nm, respectively. It is clearly evident that the sample obtained by the potentiostatic anodization (POT) shows small crystal size than that of the galvanostatic (GAL) method.

Figure 3 depicts the morphologies of nanostructures of CuO/Cu_2O investigated with scanning electron microscopy (SEM). Figures 3(a) and 3(b) exhibit coral-like CuO/Cu_2O nanorods (NRs) which are formed during the potentiostatic modes of anodization carried out at the rate of about 20 V, whereas (Figures 3(c) and 3(d)) represent high-magnification images of CuO/Cu_2O nanopolycrystals (NPCs) formed during galvanostatic modes of anodization

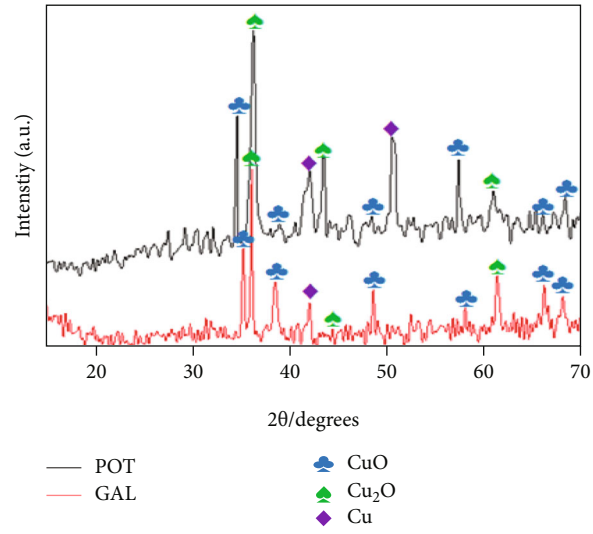

Figure 2: XRD pattern of the POT grown CuO/Cu_2O and GAL grown CuO/Cu_2O.

at the rate of about 10 mA cm^{-2}. The coral-like nanorods have a pointing tips that are around 26.9 nm and 29.3 nm presented in Figure 3(b) indicating a well-ordered morphology, demonstrating a controlled-size and rod-like structure which may help to enhance for the supercapacitor applications [48]. Figure 3(d) represents the size and shape of the CuO/Cu_2O nanopolycrystals (NPCs) that are around 50.3 nm and 57.2 nm which are in general larger in size compared to its counterpart.

The thermal stability of the nanomaterials was determined by thermogravimetry and differential thermal analysis (TG/DTA). The TG/DTA traces of CuO/Cu_2O nanoparticles are shown in (Figure 4). A small weight loss appears room temperature to 100°C recognized due to dehydration of

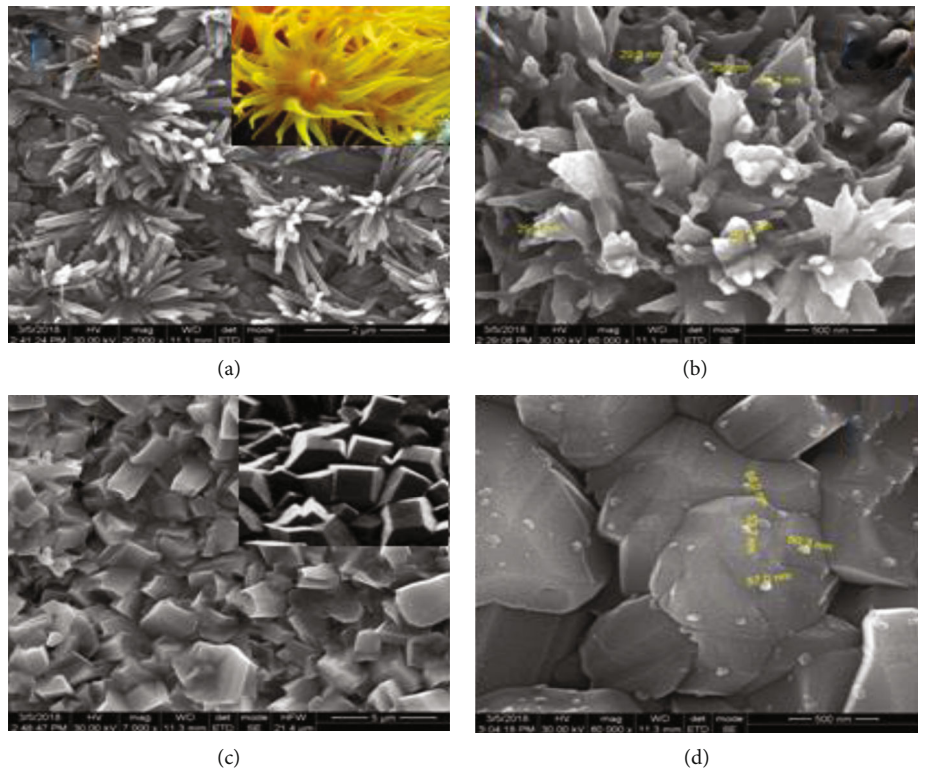

Figure 3: The high magnification SEM images of (a, b) POT grown CuO/Cu_2O (NRs) and (c, d) GAL grown CuO/Cu_2O (NPCs).

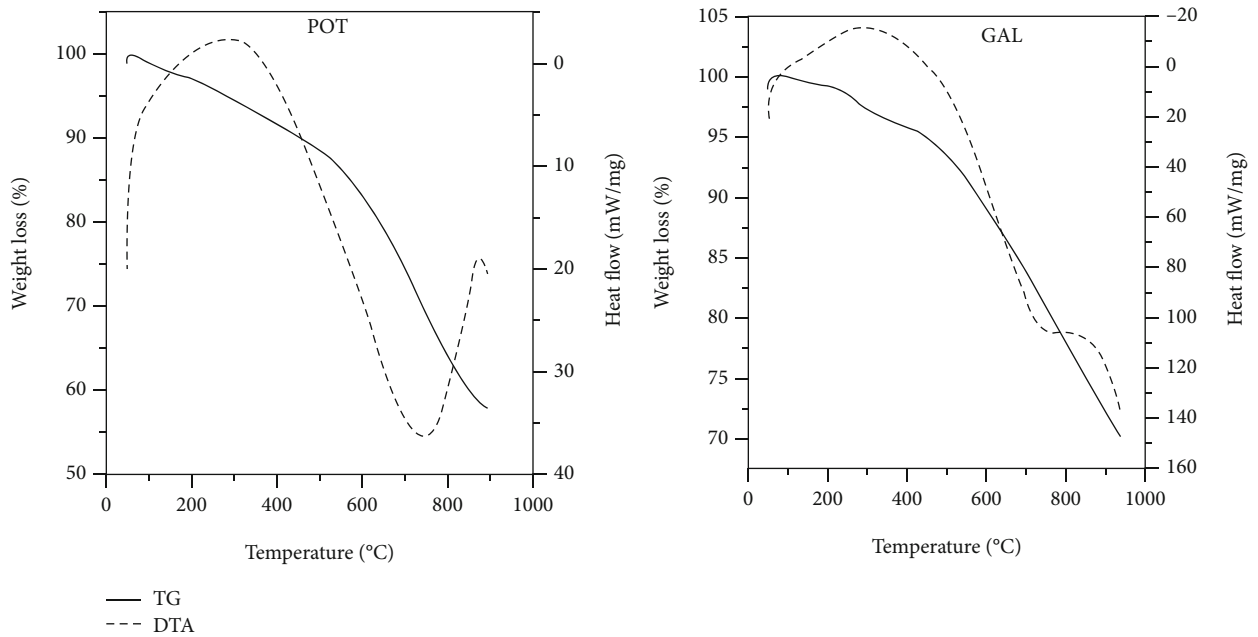

Figure 4: TG/DTA of CuO/Cu_2O for potentiostatic (POT) and galvanostatic (GAL) modes.

surface moisture. The POT samples gradually lose weight but is almost stable until 600°C with an estimated weight loss of 10%; on the other hand, GAL depicted a weight loss of 5% at 200°C and another 5% at 500°C and a slope nearing 20% at 600°C. From the TG graphs, it is clearly evident that the POT route synthesized samples were more stable at higher temperature than the GAL route.

FT-IR spectra of the CuO/Cu_2O nanostructures prepared in different modes are shown in (Figure 5). The broad absorption peaks at 3444 cm^{-1} and 3437 cm^{-1} belong to the

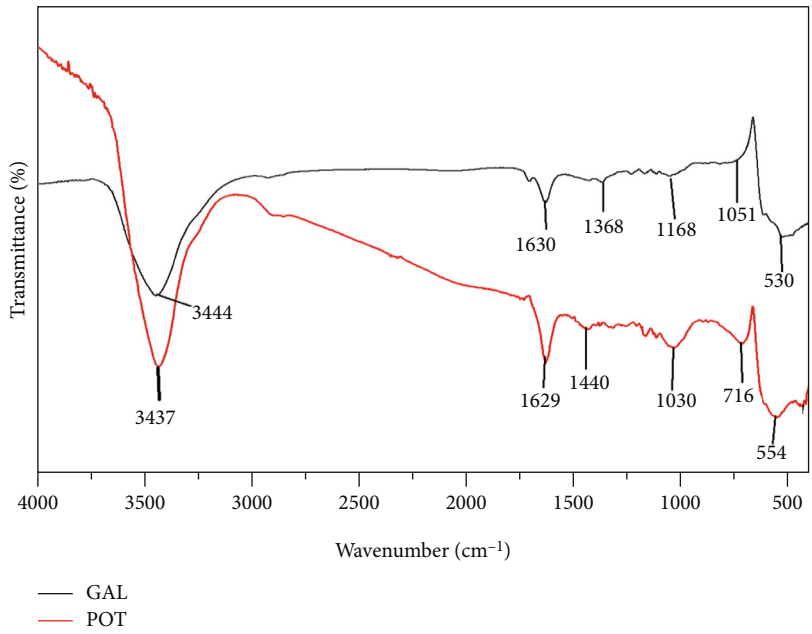

Figure 5: FT-IR spectra of CuO/Cu_2O NRs and NPCs prepared using different modes.

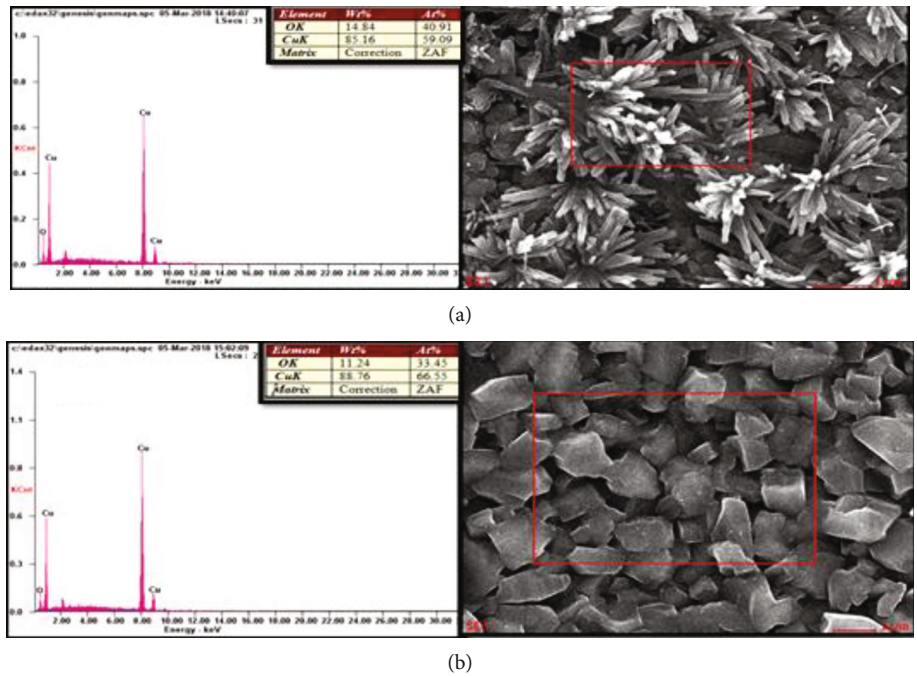

Figure 6: EDX spectra with SEM images of CuO/Cu_2O NRs and NPCs developed using different modes: (a) POT and (b) GAL.

symmetric or asymmetric stretching of O-H bonds. The peaks were observed at 1630 cm^{-1} and 1629 cm^{-1} indicate the formation of CuO nanoparticles. The stretching vibration of Cu-O bonds of Cu_2O nanoparticles is found at 1100-1400 $cm^{-1}$and shown in (Figure 5). The two infrared absorption peaks reveal the vibrational modes in the range of 500-700 cm^{-1}. The peaks observed at 530 cm^{-1} represent the formation of CuO/Cu_2O (NRs) and 554 cm^{-1} for $CuO/-Cu_2O$ (NPCs), respectively. Therefore, the metal-oxygen frequencies observed for CuO nanoparticles are in close agreement with those reported in the literature. Figure 6 shows the energy dispersive X-ray (EDX) analysis of POT (NRs) and GAL (NPCs) annealed at 350°C for 1 hr. Graphical representation reveals the presence of copper (Cu) and oxygen (O) elements in nanoparticals, and the data indicate that the nanocomposites are nearly stoichiometric. The weight percent of copper and oxide calculated from EDX analysis is shown in Figures 6(a) and 6(b). No other

Table 1: Comparison of research approaches and findings.

Substrate	Electrolyte	Time (min)	Morphology	Current/potential applied	References
Cu foil	2 M KOH	15	Nanowires	2.5 mA/cm^2	[49]
Cu foam	3 M KOH	20	Leaf-like	30 mA/cm^2	[37]
Cu foam	3 M KOH	30	Nanosheets	20 mA/cm^2	[50]
Cu foil	3 M KOH	120	Flower-like	6 mA/cm^2	[51]
Cu foil	0.1-0.5 M oxalate	30	Spheres	7.5-9 V	[52]
Cu foil	$Ni(NO_3)_2{\cdot}6H_2O$ (1 M)	5		1 mA/cm^2	[53]
Cu foil	2 M KOH	20	Needle	1.3 &1.8 V	[54]
	3 M KOH	20			
Cu foil	1 M NaOH	15	Rods	20 V (POT)	This work
	1 M NaOH	15	Particles	10 mA/cm^2 (GAL)	

elemental impurities are detected in the EDX spectra. This result confirmed that the formation of *as*-prepared metal oxides was CuO/Cu_2O nanoparticals. Table 1 describes a list of materials fabricated by a similar procedure.

4. Conclusion

In this paper, we have demonstrated a facile and cost-effective potentiostatic and galvanostatic modes of the anodization method to synthesize the coral-like CuO/Cu_2O nanorods and CuO/Cu_2O nanopolycrystals on copper foil. Fascinatingly, the comparative studies from the XRD patterns revealed that the galvanostatically anodized CuO/-Cu_2O NPCs have a chaotic structure and large crystallite size on comparison with POT mode, whereas potentiostatically anodized coral-like NRs have a well-layered structure and binder less and smaller crystallite size as compared to the galvanostatic technique from HRSEM analysis. The thermal studies indicate that the POT mode fabricated samples were found to be more stable than the GAL mode. EDX analysis depicted a higher purity of both the samples.

Data Availability

The data supporting this work is available from the corresponding author upon request.

Conflicts of Interest

The authors declare that they have no conflicts of interest.

References

[1] P. Xu, J. Liu, T. Liu et al., "Preparation of binder-free CuO/Cu_2O/cu composites: a novel electrode material for supercapacitor applications," *RSC Advances*, vol. 6, no. 34, pp. 28270–28278, 2016.

[2] T. Zhu, S. Zheng, Y. Lu, Y. Chen, Y. Chen, and H. Guo, "Influence of iron concentration and post-annealing temperature on structure and pseudocapacitive characteristics of a MnO_2–Fe_2O_3 nanocomposite," *Journal of Solid State Electrochemistry*, vol. 19, no. 2, pp. 381–390, 2015.

[3] Q. Yu, H. Huang, R. Chen et al., "Synthesis of CuO nanowalnuts and nanoribbons from aqueous solution and their catalytic and electrochemical properties," *Nanoscale*, vol. 4, no. 8, pp. 2613–2620, 2012.

[4] X. Peng, J. Jin, Y. Nakamura, T. Ohno, and I. Ichinose, "Ultrafast permeation of water through protein-based membranes," *Nature Nanotechnology*, vol. 4, no. 6, pp. 353–357, 2009.

[5] H. Huang, Q. Yu, X. Peng, and Z. Ye, "Mesoporous protein thin films for molecule delivery," *Journal of Materials Chemistry*, vol. 21, no. 35, pp. 13172–13179, 2011.

[6] X. Peng, Q. Yu, Z. Ye, and I. Ichinose, "Flexible ultrathin free-standing fluorescent films of $CdSe_xS_1$– x/ZnS nanocrystalline and protein," *Journal of Materials Chemistry*, vol. 21, no. 12, pp. 4424–4431, 2011.

[7] X. Peng, J. Jin, E. M. Ericsson, and I. Ichinose, "General method for ultrathin free-standing films of nanofibrous composite materials," *Journal of the American Chemical Society*, vol. 129, no. 27, pp. 8625–8633, 2007.

[8] J. Li, W. Cao, Y. Mao, Y. Ying, L. Sun, and X. Peng, "Zinc hydroxide nanostrands: unique precursors for synthesis of ZIF-8 thin membranes exhibiting high size-sieving ability for gas separation," *CrystEngComm*, vol. 16, no. 42, pp. 9788–9791, 2014.

[9] H.-P. Cong, X.-C. Ren, P. Wang, and S.-H. Yu, "Flexible graphene–polyaniline composite paper for high-performance supercapacitor," *Energy & Environmental Science*, vol. 6, no. 4, pp. 1185–1191, 2013.

[10] C. M. Magdalane, K. Kaviyarasu, M. V. Arularasu, K. Kanimozhi, and G. Ramalingam, "Structural and morphological properties of Co_3O_4 nanostructures: investigation of low temperature oxidation for photocatalytic application for waste water treatment," *Surfaces and Interfaces*, vol. 17, p. 100369, 2019.

[11] W. Wang, S. Guo, I. Lee et al., "Hydrous ruthenium oxide nanoparticles anchored to graphene and carbon nanotube hybrid foam for supercapacitors," *Scientific Reports*, vol. 4, no. 1, p. 4452, 2014.

[12] M. Wang, Y. Wang, H. Dou, G. Wei, and X. Wang, "Enhanced rate capability of nanostructured three-dimensional graphene/Ni_3S_2 composite for supercapacitor electrode," *Ceramics International*, vol. 42, no. 8, pp. 9858–9865, 2016.

[13] M. Huang, F. Li, Y. X. Zhang, B. Li, and X. Gao, "Hierarchical NiO nanoflake coated CuO flower core-shell nanostructures for supercapacitor," *Ceramics International*, vol. 40, no. 4, pp. 5533–5538, 2014.

[14] G. Wang, J. Huang, S. Chen, Y. Gao, and D. Cao, "Preparation and supercapacitance of CuO nanosheet arrays grown on nickel foam," *Journal of Power Sources*, vol. 196, no. 13, pp. 5756–5760, 2011.

[15] Y. Li, S. Chang, X. Liu et al., "Nanostructured CuO directly grown on copper foam and their supercapacitance performance," *Electrochimica Acta*, vol. 85, pp. 393–398, 2012.

[16] G. Ramalingam, R. Vignesh, C. Ragupathi, C. M. Magdalane, K. Kaviyarasu, and J. Kennedy, "Electrical and chemical stability of CuS nanofluids for conductivity of water soluble based nanocomposites," *Surfaces and Interfaces*, vol. 19, p. 100475, 2020.

[17] P. Surendran, A. Lakshmanan, S. Sakthy Priya et al., "Optical and nonlinear optical properties of $Zn_{0.96}Cu_{0.04}Al_2O_4$ nanocomposites prepared by combustion method," *Materials Today: Proceedings*, vol. 36, pp. 175–178, 2020.

[18] A. Lakshmanan, P. Surendran, S. SakthyPriya et al., "Effect of fuel content on nonlinear optical and antibacterial activities of $Zn/cu/Al_2O_4$ nanoparticles prepared by microwave-assisted combustion method," *J. King Saud Univ. - Sci.*, vol. 32, no. 2, pp. 1382–1389, 2020.

[19] B. Arjunkumar, G. Ramalingam, M. Ramesh, J. S. Ponraj, and K. V. Rao, "Investigation of uni-directional nanorods composed microspheres and branched TiO_2 nanorods towards solar cell application," *Materials Letters*, vol. 273, p. 127900, 2020.

[20] R. Gopal, M. M. Chinnapan, A. K. Bojarajan et al., "Facile synthesis and defect optimization of 2D-layered MoS_2 on TiO_2 heterostructure for industrial effluent, wastewater treatments," *Scientific Reports*, vol. 10, no. 1, p. 21625, 2020.

[21] F. Beshkar, H. Khojasteh, and M. Salavati-Niasari, "Recyclable magnetic superhydrophobic straw soot sponge for highly efficient oil/water separation," *Journal of Colloid and Interface Science*, vol. 497, pp. 57–65, 2017.

[22] S. Mortazavi-Derazkola, M. Salavati-Niasari, O. Amiri, and A. Abbasi, "Fabrication and characterization of Fe_3O_4@-SiO_2@TiO_2@Ho nanostructures as a novel and highly efficient photocatalyst for degradation of organic pollution," *Journal of Energy Chemistry*, vol. 26, no. 1, pp. 17–23, 2017.

[23] J. Huang, H. Wu, D. Cao, and G. Wang, "Influence of Ag doped CuO nanosheet arrays on electrochemical behaviors for supercapacitors," *Electrochimica Acta*, vol. 75, pp. 208–212, 2012.

[24] M. Zhi, C. Xiang, J. Li, M. Li, and N. Wu, "Nanostructured carbon–metal oxide composite electrodes for supercapacitors: a review," *Nanoscale*, vol. 5, no. 1, pp. 72–88, 2013.

[25] W. Zhang, M. Li, Q. Wang et al., "Hierarchical Self-assembly of Microscale Cog-like Superstructures for Enhanced Performance in Lithium-Ion Batteries," *Advanced Functional Materials*, vol. 21, no. 18, pp. 3516–3523, 2011.

[26] D. P. Volanti, M. O. Orlandi, J. Andrés, and E. Longo, "Efficient microwave-assisted hydrothermal synthesis of CuO sea urchin-like architectures via a mesoscale self-assembly," *CrystEngComm*, vol. 12, no. 6, pp. 1696–1699, 2010.

[27] X. Wang, C. Hu, H. Liu, G. Du, X. He, and Y. Xi, "Synthesis of CuO nanostructures and their application for nonenzymatic glucose sensing," *Sensors and Actuators B: Chemical*, vol. 144, no. 1, pp. 220–225, 2010.

[28] H. Chen, J.-H. Lee, Y.-H. Kim et al., "Metallic copper nanostructures synthesized by a facile hydrothermal method," *Journal of Nanoscience and Nanotechnology*, vol. 10, no. 1, pp. 629–636, 2010.

[29] M. Veerapandian, S. Sadhasivam, J. Choi, and K. Yun, "Glucosamine functionalized copper nanoparticles: preparation, characterization and enhancement of anti-bacterial activity by ultraviolet irradiation," *Chemical Engineering Journal*, vol. 209, pp. 558–567, 2012.

[30] S. Gao, S. Yang, J. Shu, S. Zhang, Z. Li, and K. Jiang, "Green fabrication of hierarchical CuO hollow micro/nanostructures and enhanced performance as electrode materials for lithium-ion batteries," *Journal of Physical Chemistry C*, vol. 112, no. 49, pp. 19324–19328, 2008.

[31] K. Krishnamoorthy and S.-J. Kim, "Growth, characterization and electrochemical properties of hierarchical CuO nanostructures for supercapacitor applications," *Materials Research Bulletin*, vol. 48, no. 9, pp. 3136–3139, 2013.

[32] B. Y. Xia, P. Yang, Y. Sun et al., "One-Dimensional Nanostructures: Synthesis, Characterization, and Applications," *Advanced Materials*, vol. 15, no. 5, pp. 353–389, 2003.

[33] L. Wang, W. Cheng, H. Gong et al., "Facile synthesis of nanocrystalline-assembled bundle-like CuO nanostructure with high rate capacities and enhanced cycling stability as an anode material for lithium-ion batteries," *Journal of Materials Chemistry*, vol. 22, no. 22, pp. 11297–11302, 2012.

[34] Y. Cheng, Y. Lin, J. Xu et al., "Surface plasmon resonance enhanced visible-light-driven photocatalytic activity in cu nanoparticles covered Cu_2O microspheres for degrading organic pollutants," *Applied Surface Science*, vol. 366, pp. 120–128, 2016.

[35] V. Scuderi, G. Amiard, S. Boninelli et al., "Photocatalytic activity of CuO and Cu_2O nanowires," *Materials Science in Semiconductor Processing*, vol. 42, pp. 89–93, 2016.

[36] Y. Luo, S. Li, Q. Ren et al., "Facile synthesis of flowerlike Cu2O nanoarchitectures by a solution phase route," *Crystal Growth & Design*, vol. 7, no. 1, pp. 87–92, 2007.

[37] D. He, G. Wang, G. Liu, H. Suo, and C. Zhao, "Construction of leaf-like CuO–Cu_2O nanocomposites on copper foam for high-performance supercapacitors," *Dalton Transactions*, vol. 46, no. 10, pp. 3318–3324, 2017.

[38] Y. Yang, Y. Li, and M. Pritzker, "Control of Cu_2O film morphology using potentiostatic pulsed electrodeposition," *Electrochimica Acta*, vol. 213, pp. 225–235, 2016.

[39] X. Wen, W. Zhang, S. Yang, Z. R. Dai, and Z. L. Wang, "Solution phase synthesis of Cu(OH)2Nanoribbons by coordination self-assembly using Cu2S nanowires as precursors," *Nano Letters*, vol. 2, no. 12, pp. 1397–1401, 2002.

[40] C.-H. Tsai, P.-H. Fei, and C.-H. Chen, "Investigation of coral-like Cu2O nano/microstructures as counter electrodes for dye-sensitized solar cells," *Materials (Basel).*, vol. 8, no. 9, pp. 5715–5729, 2015.

[41] A. Paracchino, J. C. Brauer, J.-E. Moser, E. Thimsen, and M. Graetzel, "Synthesis and characterization of high-photoactivity electrodeposited Cu2O solar absorber by photoelectrochemistry and ultrafast spectroscopy," *Journal of Physical Chemistry C*, vol. 116, no. 13, pp. 7341–7350, 2012.

[42] Y. Tan, X. Xue, Q. Peng, H. Zhao, T. Wang, and Y. Li, "Controllable fabrication and electrical performance of single crystalline Cu2O nanowires with high aspect ratios," *Nano Letters*, vol. 7, no. 12, pp. 3723–3728, 2007.

[43] R. V. Kumar, Y. Mastai, Y. Diamant, and A. Gedanken, "Sonochemical synthesis of amorphous cu and nanocrystalline

Cu2O embedded in a polyaniline matrix," *Journal of Materials Chemistry*, vol. 11, no. 4, pp. 1209–1213, 2001.

[44] N. G. Elfadill, M. R. Hashim, K. M. Chahrour, and S. A. Mohammed, "Electrochemical deposition of Na-doped p-type Cu_2O film on n-type Si for photovoltaic application," *Journal of Electroanalytical Chemistry*, vol. 767, pp. 7–12, 2016.

[45] A. Osherov, C. Zhu, and M. J. Panzer, "Influence of ITO electrode surface composition on the growth and optoelectronic properties of electrodeposited Cu2O thin films," *Journal of Physical Chemistry C*, vol. 117, no. 47, pp. 24937–24942, 2013.

[46] N. K. Allam and C. A. Grimes, "Formation of vertically oriented TiO2 nanotube arrays using a fluoride free HCl aqueous electrolyte," *Journal of Physical Chemistry C*, vol. 111, no. 35, pp. 13028–13032, 2007.

[47] R. S. Hyam, J. Lee, E. Cho, J. Khim, and H. Lee, "Synthesis of copper hydroxide and oxide nanostructures via anodization technique for efficient photocatalytic application," *Journal of Nanoscience and Nanotechnology*, vol. 12, no. 11, pp. 8396–8400, 2012.

[48] S. Zhao, T. Liu, Y. Zhang et al., "Cr-doped MnO_2 nanostructure: morphology evolution and electrochemical properties," *Journal of Materials Science: Materials in Electronics*, vol. 27, no. 4, pp. 3265–3270, 2016.

[49] J. Zhao, X. Shu, Y. Wang et al., "Construction of CuO/Cu_2@-CoO core shell nanowire arrays for high-performance supercapacitors," *Surface and Coatings Technology*, vol. 299, pp. 15–21, 2016.

[50] J. Bai, L. Yang, B. Dai et al., "Synthesis of CuO-Cu_2@graphene nanosheet arrays with accurate hybrid nanostructures and tunable electrochemical properties," *Applied Surface Science*, vol. 452, pp. 259–267, 2018.

[51] P. V. Dat and N. X. Viet, "Facile synthesis of novel areca flower like Cu_2O nanowire on copper foil for a highly sensitive enzyme-free glucose sensor," *Materials Science and Engineering: C*, vol. 103, p. 109758, 2019.

[52] M. H. Mahmood, Suryanto, M. H. F. al Hazza, and F. I. Haider, "Influence of Oxalate Concentration and Temperature on the Microstructure Morphology of Nano Anodized Copper Coating," *Journal of Materials Science and Engineering A*, vol. 8, no. 4, pp. 155–165, 2018.

[53] X. Shu, Y. Wang, Y. Qin et al., "Synthesis and supercapacitive performance of CuO/Cu_2O nanosheet arrays modified by hydrothermal deposited NiOOH," *Journal of Solid State Electrochemistry*, vol. 21, no. 5, pp. 1489–1497, 2017.

[54] L. C. T. Shoute, K. M. Alam, E. Vahidzadeh et al., "Effect of morphology on the photoelectrochemical performance of nanostructured Cu_2O photocathodes," *Nanotechnology*, vol. 32, no. 37, p. 374001, 2021.